Earth, Planets and Space

EXPRESS LETTER

Using improved Swarm's experimental absolute vector mode data to produce a candidate Definitive Geomagnetic Reference Field (DGRF) 2015.0 model

Pierre Vigneron[1], Gauthier Hulot[1*], Jean-Michel Léger[2] and Thomas Jager[2]

Abstract

We describe the way a global model of the geomagnetic field has been built using vector field data acquired by the absolute scalar magnetometers (ASM) running in vector mode on board the Alpha and Bravo satellites of the European Space Agency (ESA) Swarm mission. This model has been used as a parent model to build a candidate Definitive Geomagnetic Reference Field (DGRF) 2015.0 model to meet the call issued in the context of the recent update of the International Geomagnetic Reference Field (IGRF thirteenth generation). Because small but systematic issues were identified in a previous candidate IGRF 2015.0 model built in the same spirit (also only relying on ASM vector field data) in the context of the previous IGRF update (IGRF twelfth generation), we now also use improved ASM vector field (ASM-V) data. The issue originally affecting the ASM-V data is described, together with the way the improved data are now being produced. The resulting candidate DGRF 2015.0 model is shown to considerably improve on the previous candidate IGRF 2015.0 model (being closer to the final DGRF 2015.0 model by one order of magnitude in spherical harmonic spectral terms). It is also shown to stand among the candidate models closest to the final official DGRF 2015.0 model. Being the only candidate DGRF 2015.0 model entirely and only relying on such ASM-V data, it demonstrates the value of the new ASM-V data for such global geomagnetic field modeling purposes.

Keywords: Geomagnetism, Magnetic field modeling, IGRF, Swarm mission, Absolute vector magnetometers

Introduction

The International Geomagnetic Reference Field (IGRF) model is a set of snapshot models describing the large-scale, time-varying portion of Earth's internal magnetic field since 1900 AD. Updated every 5 years, IGRF also comes with a predictive model linearly extrapolating the field evolution until its next update. These models are massively used for a growing range of applications (see, e.g., Macmillan and Finlay 2011).

The latest IGRF update occurred in 2020 (IGRF thirteenth generation, Alken et al. 2021a). It involved the release of a definitive 2015.0 model (DGRF 2015.0), of a model for epoch 2020.0 (IGRF 2020.0) and of a predictive model for the 2020–2025 period. Each of these new models were produced under the auspices of the International Association of Geomagnetism and Aeronomy (IAGA) based on, and after evaluation of, proposed candidate models that had to be submitted by October 1, 2019.

Here, our main purpose is to report on the way one of the DGRF 2015.0 candidate models was produced, only using experimental ASM-V data (Léger et al. 2015; Fratter et al. 2016, see also below) acquired from the absolute magnetometers (ASM) on board two of the three satellites of the ESA Swarm mission (Friis-Christensen

*Correspondence: gh@ipgp.fr
[1] Université de Paris, Institut de Physique du Globe de Paris, CNRS, 75005 Paris, France
Full list of author information is available at the end of the article

et al. 2006). In addition, however, we also report on some recent improvements made in the way these ASM-V data have been produced, which the derived candidate DGRF candidate model could successfully take advantage of.

In what follows, we first recall previous successes in building geomagnetic field models based on experimental ASM-V data, stress the issues met and explain how these have led to improvement in the ASM-V data production. We next describe the way we built a parent model using these improved ASM-V data, detailing data selection procedures as well as model parameterization and optimization. We also explain how our DGRF 2015.0 candidate model was inferred from the parent model and describe the procedure used to infer error estimates provided with the candidate model. Finally, we assess and discuss the quality of our model, highlighting the benefit brought by the improved way ASM-V data are now being produced.

Early ASM-V data-based modeling success and observed limitations

Each Swarm satellite carries a vector field magnetometer (VFM) and a three-head Star Tracker (STR) collocated on an optical bench, as well as an absolute scalar magnetometer (ASM). All instruments are located on a boom away from the body of the satellite to avoid magnetic perturbations. The optical bench (with VFM and STR) stands at mid-boom, whereas the ASM is located 2 m away, at the very tip of the boom, to also avoid interferences with the VFM. The Swarm nominal Level 1b (L1b) magnetic data are produced by using relative vector field output from this VFM, calibrated using scalar output from the ASM (Tøffner-Clausen et al. 2016), and provided in both the VFM reference frame and the North East Center (NEC) reference frame. The NEC field components are inferred from synchronous readings from the STR (linking the NEC frame to its own Central Reference Frame, CRF), using calibrated Euler angles to link the CRF to the VFM frames (Olsen et al. 2013). Colocation of the VFM and STR on the same optical bench ensures stability of this CRF to VFM frame rotation. This set-up is optimal for producing nominal L1b magnetic data in the way just described, since only scalar readings (not requiring attitude transfer) from the ASM instrument are needed for calibration of the VFM.

ASM instruments, however, can also produce 1-Hz self-calibrated vector data (ASM-V data) in addition to the 1-Hz absolute scalar data nominally required by the mission (Léger et al. 2015; Fratter et al. 2016). All ASMs have near-continuously been run in this experimental vector mode since launch in November 2013 (except for the ASM on Swarm Charlie, which ceased to produce data on November 5, 2014, following a heavy ion hitting a key component of the instrument's electronics). These data are natively produced in an ASM-related reference frame, the attitude of which also needs to be transferred to the STR CRF frame for rotation of the ASM-V data in the NEC frame (using STR data) and geomagnetic field modeling purposes. Much of the ability of the ASM to produce useful ASM-V data thus depends on the mechanical stability between the tip of the boom and the optical bench. Quite remarkably, this limitation did not turn out to be critical.

ASM-V data, indeed, have already been used to successfully produce an IGRF 2015.0 candidate model (Vigneron et al. 2015) for the previous 12th generation IGRF release (Thébault et al. 2015a). This ASM IGRF 2015.0 candidate model was well evaluated at the time and contributed to the official IGRF 2015.0 model (Thébault et al. 2015b), convincingly demonstrating that ASM-V data could be used as an alternative to the nominal L1b magnetic data of the Swarm mission to produce global geomagnetic field models (see also Hulot et al. 2015).

Careful comparisons with a twin model produced in exactly the same way as the ASM IGRF 2015.0 candidate model (using identical data distributions and modeling procedures), but relying on nominal L1b data, nevertheless revealed some systematic disagreements between models (see figure 5a in Vigneron et al. 2015). A weaker (up to 3 nT) but similar effect was later found when comparing more advanced twin models (see figure 2f in Hulot et al. 2015). These disagreements were attributed to possible deformations of the boom between the ASM and the optical bench. But later tests by Vigneron et al. (2018) and Vigneron (2019) revealed that such deformations could not account for the observed zonal magnetic latitude dependence of the planetary signature of these disagreements. Rather, they pointed out at a systematic issue with the ASM-V data themselves, the cause of which has now been identified.

Improving Swarm's experimental ASM-V data

To fully understand the calibration procedure of the ASM-V data, the issue affecting it and the way it has been handled, we first recall key aspects of the way the ASM operates in vector mode (for more details, see Gravrand et al. 2001; Léger et al. 2015; Fratter et al. 2016 and references therein).

The ASM is first and foremost a scalar absolute "frequency to field" converter where the measurement of the ambient field intensity B_0 is achieved thanks to a magnetic resonance experiment performed on ^{4}He atoms in a gas cell. Measurements rely on the Zeeman splitting of the three sub-levels of the 2^3S_1 metastable state of these atoms, and on the electronic magnetic resonance between these sub-levels, excited by a radio frequency

(RF) signal and amplified by a selective optical pumping process. First a high-frequency (HF) discharge is applied on the ^{4}He cell to populate the 2^3S_1 metastable state. Then a selective optical pumping is performed with a linearly polarized laser light tuned on the D_0 line (corresponding to the 2^3S_1–2^3P_0 transition), to produce disequilibrium between electronic populations of the three 2^3S_1 Zeeman sub-levels. The RF excitation signal is finally applied on the ^{4}He atoms thanks to a pair of coils. When the RF frequency is such that resonance occurs, electrons are redistributed among the three 2^3S_1 Zeeman sub-levels. This resonance is detected using the absorption signal in the transmitted pumping light, which allows the frequency f_{RF} of the RF signal to be locked on the Larmor frequency f_{Larmor} corresponding to the energy splitting between the Zeeman sub-levels. Since $f_{\mathrm{Larmor}} = \gamma_{^4\mathrm{He}} B_0/(2\pi)$, where $\gamma_{^4\mathrm{He}} \approx 28$ GHz/T is the ^{4}He gyromagnetic ratio for ^{4}He in the 2^3S_1 state, this allows B_0 to be inferred in absolute physical units from f_{RF} through $B_0 = 2\pi f_{\mathrm{RF}}/\gamma_{^4\mathrm{He}}$. This is achieved at a 10-kHz rate.

The previous set-up is further optimized to operate in an isotropic way (to maintain performance independently of the direction of the field to be measured). This requires the linear polarizations of both the pumping light and the RF excitation field to be kept close to orthogonal to the direction of the field. This is achieved thanks to a specific sensor head configuration whereby a rotor part sustaining the linear polarizer and the pair of RF coils can be rotated in a stator part (fixed with respect to the satellite) using an amagnetic piezoelectric motor (cf. Guttin et al. 1994; Jager et al. 2010).

To produce ASM-V data in vector mode, the previous high-frequency absolute scalar ASM set-up is next completed with three orthogonal sets of coils (on the stator) that produce well-controlled magnetic modulations at known frequencies. The idea is to take advantage of the high scalar bandwidth of the instrument so that the field components can be retrieved from the analysis of the high-rate and high-bandwidth scalar internal data when vector modulations imposed by the set of coils are superimposed to the ambient field sensed by the ^{4}He atoms. Vector field modulations are applied at three frequencies f_{m_i} (where $i = x, y, z$ identifies the three reference orthogonal orientations of the coils) around 8, 11 and 13 Hz and modulation amplitudes b_{m_i} of about 50 nT.

Amplitudes h_i of the modulations produced at frequencies f_{m_i} by the projections of the $\vec{b}_{m_i}$ vector modulations on the ambient field $\vec{B}_0$ can then be extracted from the high-frequency scalar measurement $B_{0\mathrm{ASM}}$ using various synchronous detection and filter stages. These h_i amplitudes are the quantities used to reconstruct the components of the vector field $\vec{B}_0$ at 1 Hz with the same low-pass filtering characteristics as the 1-Hz B_0 scalar measurements (separately and synchronously inferred from appropriate filtering of the $B_{0\mathrm{ASM}}$ signal). This is achieved using a calibration process, which so far involved:

- Temperature corrections, accounting for thermal dilatation of the coils through dilatation coefficients $\{k_{xT}, k_{yT}, k_{zT}\}$, to produce temperature-based corrected h_{i_1} amplitudes.
- Geometrical corrections, dependent on the relative orientation angle θ_{RS} between the stator and the rotor of the ASM, accounting for small relative geometrical imperfections between stator and rotor, through specific parameters $\left(k_{\theta_{\mathrm{RS}}1i},\ k_{\theta_{\mathrm{RS}}2i},\ k_{\theta_{\mathrm{RS}}3i}\right)_{i=x,y,z}$, to produce further corrected h_{i_2} amplitudes.
- Scaling and orthogonalization corrections, through vector coils scale factors $\left(\lambda_x,\ \lambda_y,\ \lambda_z\right)$ and vector coils orthogonality angles $(\alpha,\ \theta,\ \gamma)$, to convert h_{i_2} amplitudes into the final B_i estimates of the three components of the ambient field $\vec{B}_0$ in an ASM orthogonalized reference frame (linked to the stator).

Except for the k_{iT} coefficients (characterized before launch), all the above parameters can be estimated on a daily basis (to account for long-term evolution of the sensor thermal environment), using a calibration algorithm that minimizes the residual between the scalar field measurement B_0 and the modulus $\vec{B}_0$ of the reconstructed vector field $\vec{B}_0$ (Gravrand et al. 2001). This reconstruction process is summarized in Fig. 1.

Given the ASM vector mode principle, the resolution of the reconstructed vector field vector is expected to vary as a function of B_0/b_{m_i}. In orbit, it ranges from 0.7 to 2.2 nT/$\sqrt{\mathrm{Hz}}$, with a mean value of 1.6 nT/$\sqrt{\mathrm{Hz}}$. Furthermore, and as checked during qualification, vector field measurements are offset-free. In-flight daily orbital stability of the scalar residual was indeed found to be within the expected performance (Léger et al. 2015; Fratter et al. 2016).

However, the findings reported in the previous section pointed out at an issue with the ASM-V data produced in this way. This issue could not be revealed by shear inspection of the scalar residuals. It required a thorough assessment of the overall principle of ASM-V vector data production. Its cause lies in residual distortion effects inherent to the ASM scalar magnetic field control loop locking the f_{RF} frequency of the RF excitation signal to the Larmor frequency, f_{Larmor}.

This effect arises because of the combination of, first, a slight non-linearity of the dispersive resonance signal used to lock the high-bandwidth scalar frequency, and second, a small delay in the tracking of the vector modulation frequencies due to the internal control loop

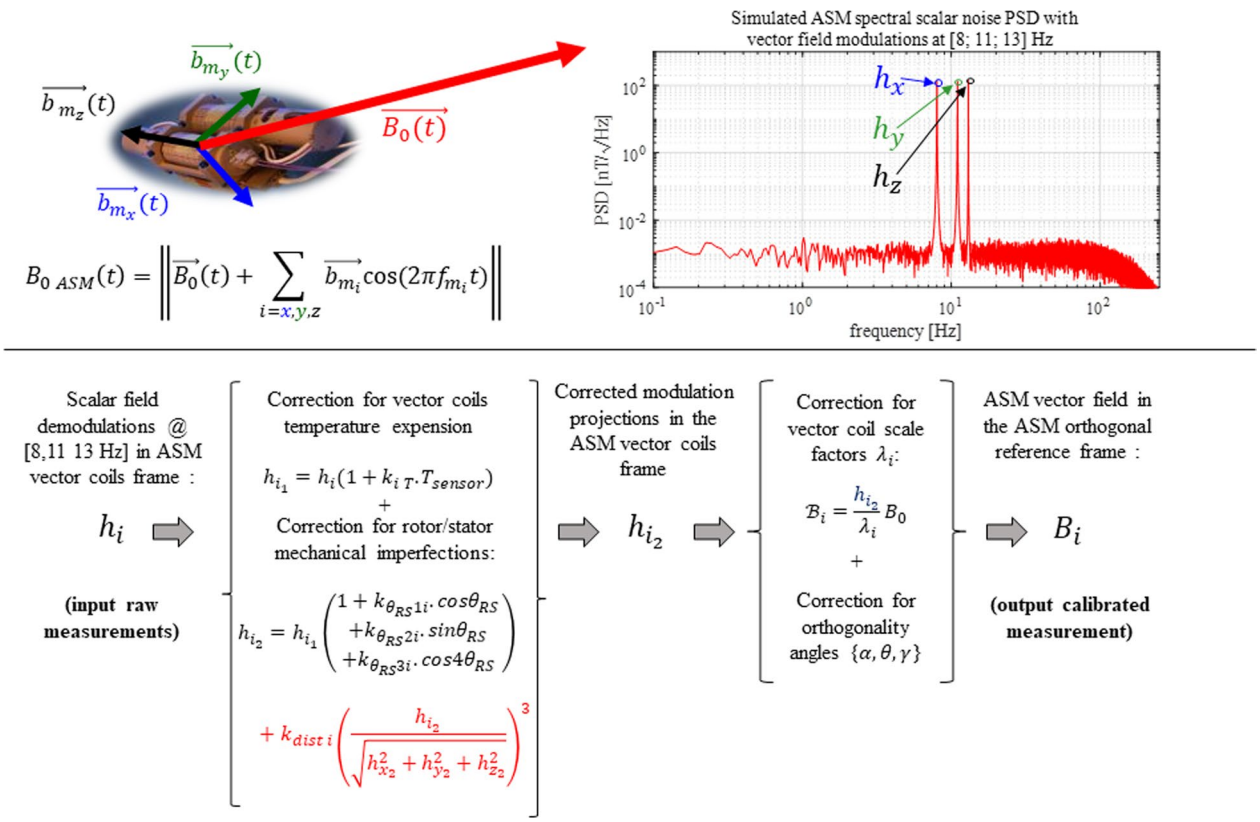

Fig. 1 Principle of the calibration process for the ASM-V data. In red, the additional correction introduced to correct for the issue now identified (see Eq. 1 in main text)

filtering characteristics. This causes a small portion of the h_i signals at 8, 11 and 13 Hz to be translated into higher odd harmonics. For a given vector field modulation, the effect is maximum when the ambient field is aligned with the modulation direction and is null when perpendicular. This effect has been modeled and corrected for to first order by introducing distortion corrections Δh_i to the h_{i_2} values (see Fig. 1):

$$\Delta h_i = k_{\mathrm{dist}i}\left(\frac{h_{i_2}}{\sqrt{h_{x_2}^2 + h_{y_2}^2 + h_{z_2}^2}}\right)^3 \quad (1)$$

where $k_{\mathrm{dist}i}$ are coefficients accounting for the non-linearity characteristics of the resonance error signal, the internal scalar RF frequency control loop filtering characteristics and the frequency of the vector modulation of interest.

The $k_{\mathrm{dist}i}$ parameters cannot be co-estimated during the calibration procedure, and must be inferred independently. This was done by relying on an ASM still available within the CEA-Leti premises, and using the observed odd harmonics of the h_i signals. Only minor additional changes to the $k_{\mathrm{dist}\,i}$ values inferred in this way (multiplication by 1.22 and 1.27, respectively) were subsequently introduced to adjust to the specificities of the Alpha and Bravo ASMs, using appropriate trial comparisons of ASM-V data with nominal Level 1b data (vector data comparisons in the NEC frame, as well as field model comparisons).

All ASM-V data used in this letter have been corrected for this effect and recalibrated, using the $k_{\mathrm{dist}i}$ parameters recovered as just described, the dilatation coefficients $\{k_{xT}, k_{yT}, k_{zT}\}$ previously determined from ground, and optimizing all other parameters through the same calibration procedure as originally done, except for the fact that the $\{k_{\theta_{\mathrm{RS}}1y}, k_{\theta_{\mathrm{RS}}2y}, k_{\theta_{\mathrm{RS}}3y}\}$ parameters (corresponding to the Y axis, weakly excited in orbit) were set to zero, as these were found to be poorly relevant in practice.

Parent and twin parent model construction

We now describe the way we built the parent model of our DGRF 2015.0 candidate model, using the improved Swarm ASM-V data. Following Vigneron et al. (2015) and Hulot et al. (2015), this approach was also designed so that a twin parent model using exactly the same data

distribution, parameterization (and damping parameters values), but relying on nominal L1b data (rather than ASM-V data) could be built.

Data selection

Only Swarm Alpha and Bravo data produced from the ASMs running in vector mode were used. ASM Level 0 data version 0201 were processed into ASM-V Level 1a data using v7 version software, and into ASM-V L1b data with UTC time stamps, using XPh1B software, stray field corrections from Swarm 0506/0506 nominal ASMxAUX files, and characterization and calibration data base (CCDB) files updated as a result of the modification introduced in the previous section.

These ASM-V data are expressed in the ASM reference frame. For geomagnetic field modeling purposes, they can be used in the same way as nominal L1b data (when using data expressed in the VFM reference frame, also available). This simply requires recovering attitude information from the q_NEC_CFR quaternion in 0506/0506 MAGxLR files, which we also used to recover satellite positions (radius/lat/long). Note that Euler angles defining the rotation between the ASM and STR CRF reference frames are not provided and must therefore be jointly computed with the models (see below).

Temporal coverage of the data extends from 30/11/2013 to 03/05/2019 (65 months). We did not use more recent data, as this was not deemed necessary to derive the targeted DGRF 2015.0 candidate model (for epoch 01/01/2015, recall also that candidate models had to be delivered on October 1, 2019).

The data selection criteria used were identical (except for possible thresholds when using indices, see below) to those previously used by Hulot et al. (2015), where details can be found:

- Only night-side data (Sun at least 10° below horizon).
- Magnetically quiet conditions (based on RC < 2 nT/h and Kp < 2+).
- For all (absolute) quasi-dipole (QD) latitudes above 55°, only scalar data, also requesting that $E_{m,12}$ < 0.8 mV/m.
- For all other QD latitudes, only vector data, unless the scalar residual (difference between scalar and modulus of vector) was larger than 0.3 nT, or the piezoelectric motor had been activated within 3 s of the measurement (since this may produce artifacts, Léger et al. 2015), in which case only scalar data were considered.
- Final decimation to avoid over-representation along tracks (amounting to separate data by about 30 s).

Again as in Hulot et al. (2015), a mild additional selection criteria was finally introduced to ensure that a non-spurious L1b nominal datum version 0505/0506 (from the VFM instruments, expressed in the VFM frame of reference) was available for each ASM-V datum selected, to build a VFM twin data set for comparison purposes, which we used for both deriving a VFM twin model and inferring model uncertainties (see below). This resulted in the selection of 313,601 scalar data and 1,340,172 × 3 vector data, distributed in time and latitude as illustrated in Fig. 2.

Model parameterization

The model parameterization is an evolution of that of Hulot et al. (2015), following the CHAOS-4 approach (Olsen et al. 2014) to better account for temporal evolution over more than 5 years. It involves a total of 6755 coefficients detailed as follows.

Core and lithospheric sources:

- Time-varying internal field up to degree and order 13 (included), using order-6 B-splines with a 6 months knots separation. This leads to 16 splines and $16 \times 13 \times (13 + 2) = 3120$ coefficients.
- Static internal field between degree and order 14 (included) and degree and order 45 (included). This leads to $45 \times (45 + 2) - 13 \times (13 + 2) = 1920$ coefficients.

A total of 5040 coefficients are thus used to model the internal field.

Magnetospheric sources, modeled as in Hulot et al. (2015) following Olsen et al. (2014), where details can be found (identical notations are used here):

- Remote magnetospheric sources (degree 2 zonal terms in GSM frame): $q_n^{0,\mathrm{GSM}}$ with $n = 1, 2$ (2 coefficients).

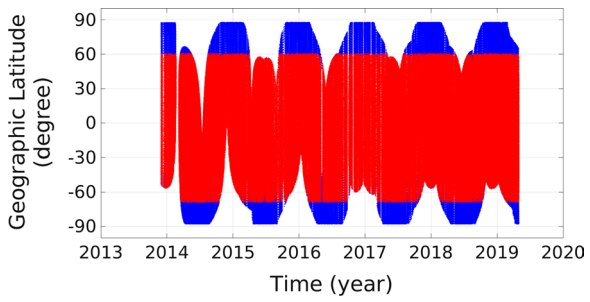

Fig. 2 Distribution of the data used to build the parent (and twin) model (as a function of time and geographic latitude; blue and partly hidden: scalar data; red: vector data)

- Near magnetospheric ring current (in SM frame): q_2^m, s_2^m for the static degree 2 (5 coefficients); $\hat{q}_1^0$, $\hat{q}_1^1$, $\hat{s}_1^1$ for the regression factors (3 coefficients); Δq_1^0 solved in bins of 5 days (395 time segments, leading to 395 coefficients), Δq_1^1 and Δs_1^1 solved in bins of 30 days (67 time segments, leading to $2 \times 67 = 134$ coefficients).

This leads to a total of $2+5+3+395+134=539$ coefficients for the external field.

Finally, Euler angles (rotation between ASM and STR reference frames) are estimated every 10 days for both satellites: 197 and 195 time segments for, respectively, Alpha and Bravo, leading to $3 \times (197 + 195) = 1176$ coefficients.

Model optimization

The model is optimized by minimizing the mismatch between data and model prediction, using iteratively reweighted least-squares with Huber weights and temporal damping as in Olsen et al. (2014) the notation of which we follow, but only using two damping parameters, λ_2 and λ_3:

- λ_2: $|\mathrm{d}^2\mathrm{B_r}/\mathrm{dt}^2|$ constrained at beginning (Nov-2013) and end (May-2019) of dataset with the same damping value as CHAOS-4 $\left[\lambda_2 = 10\left(nT\mathrm{year}^{-2}\right)^{-2}\right]$.
- λ_3: $|\mathrm{d}^3\mathrm{B_r}/\mathrm{dt}^3|$ integrated at the core surface and over the time coverage constrained with the same damping value as CHAOS-4 $\left[\lambda_3 = 0.33\left(nT\mathrm{year}^{-3}\right)^{-2}\right]$ for all Gauss coefficients except for g_1^0 where we use $\left[\lambda_3 = 10\left(nT\mathrm{yr}^{-3}\right)^{-2}\right]$.

As in Hulot et al. (2015), a geographical weight is introduced, proportional to sin (θ) (where θ is the geographic colatitude), to balance the geographical sampling of data. Anisotropic magnetic errors due to attitude uncertainty are taken into account assuming an isotropic attitude error of 10 arcsecs and the formalism of Holme and Bloxham (1996). A priori data error variances are set to 2.2 nT for both scalar and vector data. The starting model used is a static model (CHAOS-4 up to degree and order 13 only for epoch 30/11/13), but this choice was found to have no influence on the final model. A total of eight iterations were used, which was enough to ensure convergence to within the accuracy required, for both the parent and twin parent models (subsequently referred to as, respectively, the ASM-V and VFM twin parent models).

Resulting residual statistics are shown in Table 1 for both the ASM-V (left column) and VFM twin (right column) parent models, for all data (top rows), Swarm Alpha data only (middle rows) and Swarm Bravo data only (bottom rows).

DGRF 2015.0 candidate model and associated error estimates

The DGRF 2015.0 model being intended to be the best possible representation of Earth's internal magnetic field at epoch 2015.0 up to degree and order 13, and since the purpose was to produce a model only based on Swarm ASM-V data, our DGRF 2015 candidate model is simply derived from the ASM-V parent model estimated at epoch 2015.0 and truncated at degree and order 13. For comparison purposes, a twin DGRF 2015 candidate model was derived from the VFM twin parent model in the same way.

Error estimates on each of the Gauss coefficients were also produced by assuming that the main cause of errors is in the data themselves, and assessed by taking advantage of our ability to rely on VFM twin models. We first split the ASM-V data set in two: ordering and numbering data as a function of time, every even number datum is put in sub-dataset ASM-V1, every odd datum is put in sub-dataset ASM-V2. Likewise, the twin VFM data set (Swarm L1b nominal data) is split in two VFM1 and VFM2 datasets (the time distribution of VFM1/2 data matching that of ASM-V1/2). A model is next computed from each sub-dataset, using the same parameters as the parent (and twin) model, leading to four models: ASM-V1 and VFM1, ASM-V2 and VFM2. For each Gauss coefficients, the values A_1 (from ASM-V1), A_2 (from ASM-V2), V_1 (from VFM1) and V_2 (from VFM2) are next used to compute the quantity

$$\sigma = \sqrt{\frac{(A_1 - V_2)^2 + (A_2 - V_1)^2}{2}} \tag{2}$$

which we use as an error estimate for the corresponding Gauss coefficient. These error estimates, provided in addition to the DGRF 2015.0 candidate model, are consistent with the observed spectral difference between this model and its twin (shown in Fig. 3). Note, however, that this technique only provides estimates of variances and ignores possible cross-correlations between Gauss coefficients. It also ignores uncertainties due to the choice of the modeling strategy, data selection criteria and parameters used for the inversion, more prone to subjective assessment. These error estimates should thus be viewed as a lower bound of the overall errors affecting the model.

Discussion

We focus our discussion on the two main results of this study, the fact that a high-quality DGRF 2015.0 candidate model could be built from the ASM-V data, and the fact

Table 1 Residual statistics for all data used to produce the ASM-V and VFM twin parent models

		N	ASM-V (ASM-V data)		VFM twin (VFM data)	
			Mean (nT)	RMS (nT)	Mean (nT)	RMS (nT)
Alpha + Bravo	F	313,601	− 0.07	3.87	− 0.07	3.87
	F and B_B	1,653,773	+0.03	2.55	+0.01	2.53
	B_B	1,340,172	+0.05	2.19	+0.03	2.16
	B_r	1,340,172	− 0.01	2.16	− 0.01	1.55
	B_θ	1,340,172	+0.06	3.31	+0.02	2.92
	B_φ	1,340,172	− 0.01	2.86	+0.01	2.48
Alpha	F	157,073	− 0.17	3.98	− 0.18	4.00
	FandB_B	823,580	+0.01	2.60	− 0.01	2.59
	B_B	666,507	+0.05	2.21	+0.03	2.19
	B_r	666,507	+0.01	2.23	+0.01	1.58
	B_θ	666,507	+0.03	3.34	+0.03	2.93
	B_φ	666,507	− 0.01	2.88	− 0.00	2.48
Bravo	F	156,528	+0.03	3.75	+0.04	3.75
	F and B_B	830,193	+0.05	2.51	+0.03	2.48
	B_B	673,665	+0.06	2.17	+0.03	2.13
	B_r	673,665	− 0.04	2.08	− 0.04	1.51
	B_θ	673,665	+0.09	3.29	+0.01	2.91
	B_φ	673,665	− 0.01	2.84	+0.02	2.49

N is the number of data used; *mean* and *RMS* are the Huber-weighted misfit mean and root mean square values (in nT); *F* stands for scalar data; B_B stands for the field component projected along the field direction (providing a measure of the misfit of the modulus of the vector data with respect to model prediction); B_r, B_θ and B_φ stand for the three geocentric vector field components

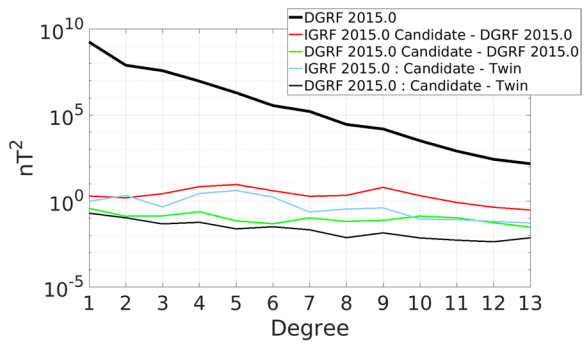

Fig. 3 Lowes–Mauersberger spectral comparison of models. Spectra of the official DGRF 2015.0 model (heavy black line) and of its difference with, respectively, the DGRF 2015.0 candidate model (green line) and IGRF 2015.0 candidate model of Vigneron et al. (2015) (red line). Also shown, spectra of the difference between the DGRF 2015.0 candidate model and its twin model (black line), and of the difference between the IGRF 2015.0 candidate model of Vigneron et al. (2015) and its twin (cyan line). All spectra are computed at Earth's surface

that the new way of producing the ASM-V data indeed removed the issues previously identified by Vigneron et al. (2015) and Hulot et al. (2015).

We first illustrate this by relying on spectral comparisons, using Lowes–Mauersberger spectra (Lowes, 1966; Mauersberger, 1956) computed at Earth's surface. Figure 3 shows the spectrum of the difference between our DGRF 2015.0 candidate model and the official DGRF 2015.0 model (in green). With values ranging between 0.4 nT^2 (for $n = 1$) and 0.03 nT^2 (for $n = 13$), this spectrum lies well below the spectrum of the official DGRF 2015.0 model (now released, Alken et al. 2021a, also shown in thick black line). As was already noted during the evaluation process of DGRF 2015.0 candidate models, this spectrum also systemically lies within the lowest range of all spectra built in the same way from all candidate models (see Fig. 1 in Alken et al. 2021b), making it one of the very best DGRF 2015.0 candidate models by this measure.

A similar comparison done between IGRF 2015.0 candidate models for the previous IGRF 12 release did not reveal such a remarkable performance of the IGRF 2015.0 candidate model built by Vigneron et al. (2015), who used the original ASM-V data. This model did not fare very well for degrees between 4 and 6 (see Fig. 4 in Thébault et al. 2015b). This already is an indication that the new way of processing ASM-V data indeed improved the quality of this data. The improvement brought by our DGRF 2015.0 candidate model compared to the IGRF 2015.0 candidate model of Vigneron et al. (2015) is illustrated in Fig. 3, which also shows the spectrum

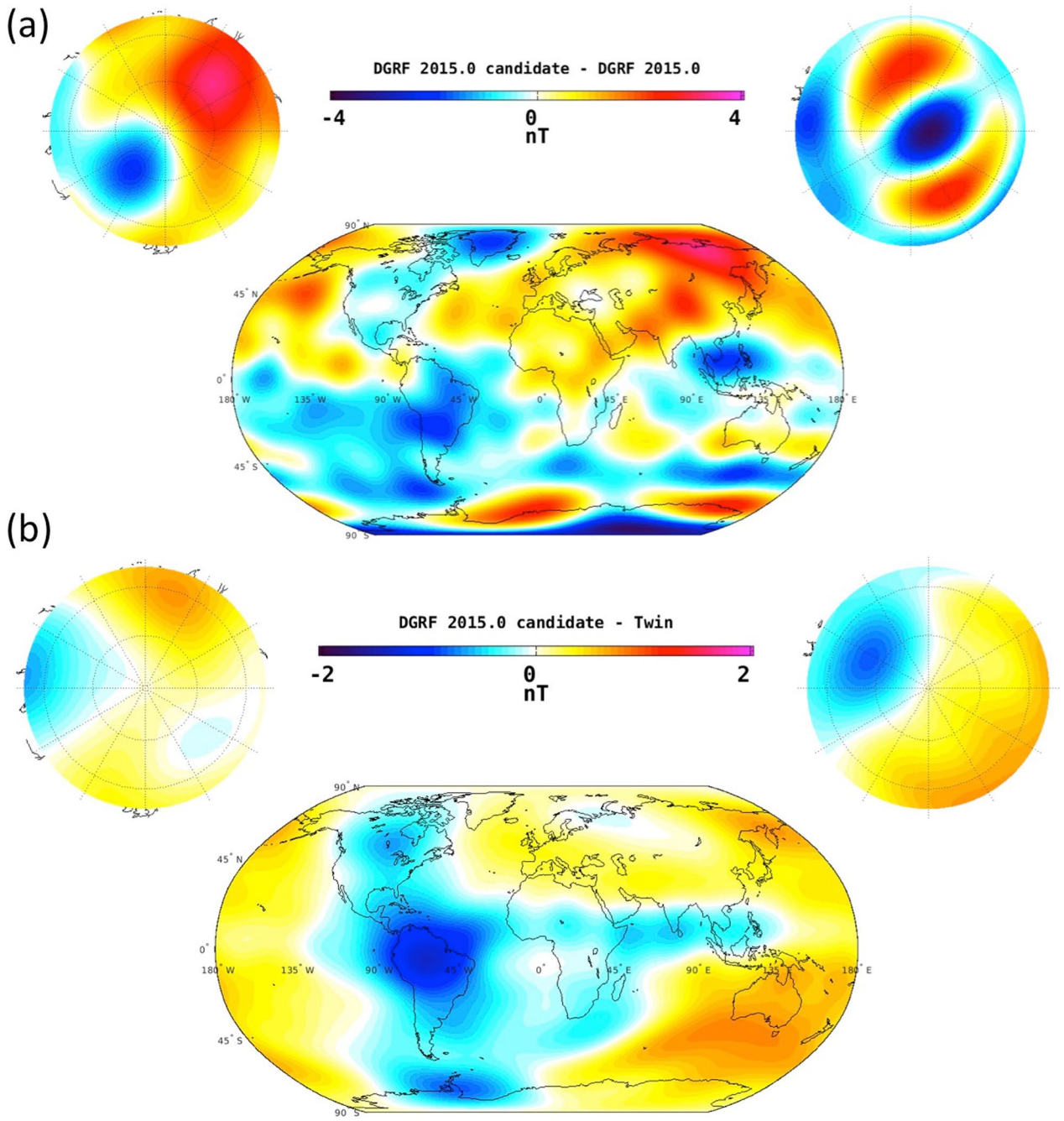

Fig. 4 Maps of the radial component B_r of the field for relevant model comparisons. **a** Difference between the DGRF 2015.0 candidate model and the official DGRF 2015.0 model. **b** Difference between the DGRF 2015.0 candidate model and its twin model. Both maps are computed at Earth's surface up to degree and order 13

of the difference between the latter model and the official DGRF 2015.0 model (in red). This spectrum lies well above the spectrum of the difference between our DGRF 2015.0 candidate model and the official DGRF 2015.0 model (in green). This improvement, however, is not just because our DGRF 2015.0 candidate model now relies on reprocessed ASM-V data. It also reflects the fact that this model is now derived from a parent model inferred from data extending up to 03/05/2019, whereas the IGRF 2015.0 candidate model of Vigneron et al. (2015) used an extrapolation of a parent model inferred from data extending only up to 25/09/2014. To better single out

the impact of the improved ASM-V data, we also plot in Fig. 3 both the spectrum of the difference between our DGRF 2015.0 candidate model and its twin DGRF 2015.0 candidate model (in black), and the spectrum of the difference between the IGRF 2015.0 candidate model of Vigneron et al. (2015) and the twin IGRF 2015.0 candidate model these authors had built in the same way, i.e. by substituting VFM data to the ASM-V data (in cyan). Each of these spectra can be viewed as a measure of how well candidate models built in the same way from either ASM-V or VFM data agree with each other. As can be seen, the agreement of our DGRF 2015.0 candidate model with its twin is much better than that of the IGRF 2015.0 candidate model with its own twin, particularly so for degrees ranging between 4 and 6. This now directly testifies for the improvement brought by the new ASM-V data.

To further illustrate the quality of our DGRF 2015.0 candidate model and the improvement brought by the ASM-V data, we now turn to maps of the radial component B_r of the field at the Earth's surface, for relevant field model differences.

Figure 4a shows a map of the difference between our DGRF 2015.0 candidate model and the official DGRF 2015.0 model. These differences lie within the $\pm$ 4 nT range, with no particularly well organized pattern, except possibly for the fact that the strongest differences tend to occur at high latitudes, where maximum differences are indeed expected to occur because of the challenge of dealing with high latitude external field contamination. As a matter of fact, and as can be seen in Fig. 3 of Alken et al. (2021b), which provides similar map comparisons for all 11 DGRF 2015.0 candidate models, our DGRF 2015.0 candidate model stands among the very few candidate models most closely matching the official DGRF 2015.0 model. This further demonstrates the increased value of the new ASM-V data. Recall indeed that our candidate model only used ASM-V data, whereas all other candidate models used nominal L1b VFM data [whenever using Swarm data, see Alken et al. (2021b) and references therein].

An additional illustration of the increased value of the new ASM-V data for global geomagnetic field modeling purposes is provided in Fig. 4b. This map of the difference between our DGRF 2015.0 candidate model and its twin illustrates the impact of using the new ASM-V data in place of the L1b VFM data, all else being equal. This leads to differences well within the 1 nT range, except in a few localized regions, such as above South America, where differences can reach 2 nT. The reason for this is unknown. It could of course be related to a remaining unidentified ASM calibration issue, but other causes may come into play, such as small distortions of the boom, or, more likely, artifacts linked to the so-called dBSun perturbations currently corrected for in the L1b VFM data by assuming that only the VFM instrument is affected (see Tøffner-Clausen et al. 2016). Yet, it is now known that part of this perturbation is also affecting the ASM instrument (Vigneron, 2019), and that this correction thus needs to be split between the VFM and ASM data. This revised way of correcting the VFM and ASM-V data will hopefully further improve and reconcile both data sets.

Notwithstanding the above remaining issue, it is worth finally stressing how successful the new way of producing the ASM-V data has been at removing all zonal artifact signatures identified by Vigneron et al. (2015) and Hulot et al. (2015). Comparing Fig. 4b with, e.g., Fig. 2f of Hulot et al. (2015) makes this very clear.

Abbreviations

ASM: Absolute scalar magnetometer; ASM-V: ASM vector field; CRF: Central reference frame; DGRF: Definitive Geomagnetic Reference Field; ESA: European Space Agency; HF: High frequency; IAGA: International Association of Geomagnetism and Aeronomy; IGRF: International Geomagnetic Reference Field; L1b: Level 1b; NEC: North East Center; QD: Quasi-dipole; RF: Radio frequency; STR: Three-head Star Tracker; VFM: Vector field magnetometer.

Acknowledgements

The authors wish to thank L. Chauvet and O. Bonnot (Geomagnetism team of IPGP) for their technical support in producing ASM-V data and making them publicly available, and two anonymous reviewers for their very helpful comments.

Authors' contributions

PV produced the ASM-V data and built the models. GH designed and led the study. He also wrote the manuscript with inputs from all authors. J-ML and TJ designed and built the ASM instruments, and designed the new way of producing ASM-V data. All authors read and approved the final manuscript.

Funding

The Swarm mission is supported by the European Space Agency (ESA), with contribution from the French Centre National des Etudes Spatiales CNES, who funded and provided as Customer Furnished Instrument the ASM instruments built by CEA-Leti. This work was supported by CNES in the framework of the program "Exploitation de la mission satellitaire européenne Swarm".

Availability of data and materials

Swarm nominal L1b data are available from https://earth.esa.int/web/guest/swarm/data-access. The experimental ASM-V data used in this study are ASMV data version 050X (0505, 0506, 0507 or 0508) produced by IPGP/CEA-Léti using the ASM CEA-Léti designed/ CNES Customer Furnished Instrument. These ASM-V data as well as the ASM-V derived models (parent model and DGRF 2015 candidate model with associated error estimates) are accessible at https://swarm.ipgp.fr/. ASM-V data are also intended to later be made available through the "Form@Ter—Data and Service for the Solid Earth" Center (https://en.poleterresolide.fr/).

Declarations

Ethics approval and consent to participate

Not applicable.

Consent for publication

Not applicable.

Competing interests
The authors declare that they have no competing interests.

Author details
[1]Université de Paris, Institut de Physique du Globe de Paris, CNRS, 75005 Paris, France. [2]Université Grenoble Alpes, CEA, Leti, 38000 Grenoble, France.

Received: 8 July 2021 Accepted: 6 October 2021
Published online: 25 October 2021

References

Alken P, Thébault E, Beggan C, Amit H, Aubert J, Baerenzung J, Bondar TN, Brown W, Cali S, Chambodut A, Chulliat A, Cox G, Finlay CC, Fournier A, Gillet N, Grayver A, Hammer M, Holschneider M, Huder L, Hulot G, Jager T, Kloss C, Korte M, Kuang W, Kuvshinov A, Langlais B, Léger J-M, Lesur V, Livermore PW, Lowes FJ, Macmillan S, Magnes W, Mandea M, Marsal S, Matzka J, Metman MC, Minami T, Morschhauser A, Mound JE, Nair M, Nakano S, Olsen N, Pavon-Carrasco FJ, Petrov VG, Ropp J, Rother M, Sabaka TJ, Sanchez S, Saturnino D, Schnepf N, Shen X, Stolle C, Tangborn A, Tøffner-Clausen L, Toh H, Torta JM, Varner J, Vigneron P, Vervelidou F, Wardinski I, Wicht J, Woods A, Yang Y, Zeren Z, Zhou B (2021a) International Geomagnetic Reference Field: the thirteenth generation. Earth Planets Space 73:49. https://doi.org/10.1186/s40623-020-01288-x

Alken P, Thébault E, Beggan C, Aubert J, Baerenzung J, Brown W, Cali S, Chulliat A, Cox G, Finlay CC, Fournier A, Gillet N, Hammer MD, Holschneider M, Hulot G, Korte M, Lesur V, Livermore P, Lowes F, Macmillan S, Nair M, Olsen N, Ropp G, Rother M, Schnepf NR, Stolle C, Toh H, Vervelidou F, Vigneron P, Wardinski I (2021b) Evaluation of candidate models for the 13th International Geomagnetic Reference Field. Earth Planets Space 73:48. https://doi.org/10.1186/s40623-020-01281-4

Fratter I, Léger J-M, Bertrand F, Jager F, Hulot G, Brocco L, Vigneron P (2016) Swarm Absolute Scalar Magnetometers first in-orbit results. Acta Astronaut 121:76–87. https://doi.org/10.1016/j.actaastro.2015.12.025

Friis-Christensen E, Lühr H, Hulot G (2006) Swarm: a constellation to study the Earth's magnetic field. Earth Planets Space 58:351–358. https://doi.org/10.1186/BF03351933

Gravrand O, Khokhlov A, Le Mouël J-L, Léger J-M (2001) On the calibration of a vectorial ^{4}He pumped magnetometer. Earth Planets Space 53:949–958. https://doi.org/10.1186/BF03351692

Guttin C, Léger J-M, Stoeckel F (1994) An isotropic earth field scalar magnetometer using optically pumped helium 4. J De Physique IV 4:655–659. https://doi.org/10.1051/jp4:19944174

Holme R, Bloxham J (1996) The treatment of attitude errors in satellite geomagnetic data. Phys Earth Planet Int 98:221–233. https://doi.org/10.1016/S0031-9201(96)03189-5

Hulot G, Vigneron P, Léger J-M, Fratter I, Olsen N, Jager T, Bertrand F, Brocco L, Sirol O, Lalanne X, Boness A, Cattin V (2015) Swarm's absolute magnetometer experimental vector mode, an innovative capability for space magnetometry. Geophys Res Lett 42:1352–1359. https://doi.org/10.1002/2014GL062700

Jager T, Léger J-M, Bertrand F, Fratter I, Lalaurie JC (2010) SWARM Absolute Scalar Magnetometer accuracy: analyses and measurement results. Proc IEEE Sensors 2010 Conf 2392–2395. https://doi.org/10.1109/ICSENS.2010.5690960

Léger J-M, Jager T, Bertrand F, Hulot G, Brocco L, Vigneron P, Lalanne X, Chulliat A, Fratter I (2015) In-flight performances of the absolute scalar magnetometer vector mode on board the Swarm satellites. Earth Planets Space 67:57. https://doi.org/10.1186/s40623-015-0231-1

Lowes FJ (1966) Mean-square values on sphere of spherical harmonic vector fields. J Geophys Res 71:2179. https://doi.org/10.1029/JZ071i008p02179

Macmillan S, Finlay C (2011) The international geomagnetic reference field. In: Mandea M, Korte M (eds) Geomagnetic observations and models, IAGA Special Sopron Book Series, vol 5. Springer, Heidelberg, pp 265–276

Mauersberger P (1956) Das mittel der energiedichte des geomagnetischen hauptfeldes an der Erdoberfläche und seine säkulare änderung. Gerl Beitr Geophys 65:207–215

Olsen N, Friis-Christensen E, Floberghagen R, Alken P, Beggan CD, Chulliat A, Doornbos E, Teixeira da Encarnação J, Hamilton B, Hulot G, van den Ijssel J, Kuvshinov A, Lesur V, Lühr H, Macmillan S, Maus S, Noja M, Olsen PEH, Park J, Plank G, Püthe C, Rauberg J, Ritter P, Rother M, Sabaka TJ, Schachtschneider R, Sirol O, Stolle C, Thébault E, Thomson AWP, Tøner-Clausen L, Velimsky J, Vigneron P, Visser PN (2013) The Swarm Satellite Constellation Application and Research Facility (SCARF) and swarm data products. Earth Planets Space 65(11):1189–1200. https://doi.org/10.5047/eps.2013.07.001

Olsen N, Lühr H, Finlay CC, Sabaka TJ, Michaelis I, Rauberg J, Tøffner-Clausen L (2014) The CHAOS-4 geomagnetic field model. Geophys J Int 197(2):815–827. https://doi.org/10.1093/gji/ggu033

Thébault E, Finlay CC, Beggan C, Alken P, Aubert J, Barrois O, Bertrand F, Bondar T, Boness A, Brocco L, Canet E, Chambodut A, Chulliat A, Coïsson P, Civet F, Du A, Fournier A, Fratter I, Gillet N, Hamilton B, Hamoudi M, Hulot G, Jager T, Korte M, Kuang W, Lalanne X, Langlais B, Léger J-M, Lesur V, Lowes FJ, Macmillan S, Mandea M, Manoj C, Maus S, Olsen N, Petrov V, Rother M, Sabaka TJ, Saturnino D, Schachtschneider R, Sirol O, Tangborn A, Taylor V, Thomson A, Tøffner-Clausen L, Vigneron P, Wardinski I, Zvereva T (2015a) International Geomagnetic Reference Field: the twelfth generation. Earth Planets Space 67:79. https://doi.org/10.1186/s40623-015-0228-9

Thébault E, Finlay CC, Alken P, Beggan C, Canet E, Chulliat A, Manoj C, Langlais B, Lesur V, Lowes FJ, Petrov M, Rother M, Schachtschneider R (2015b) Evaluation of candidate geomagnetic field models for IGRF-12. Earth Planets Space 67:112. https://doi.org/10.1186/s40623-015-0273-4

Tøffner-Clausen L, Lesur V, Olsen N, Finlay CC (2016) In-flight scalar calibration and characterisation of the Swarm magnetometry package. Earth Planets Space 68:129. https://doi.org/10.1186/s40623-016-0501-6

Vigneron P, Hulot G, Olsen N, Léger J-M, Jager T, Brocco L, Sirol O, Coïsson P, Lalanne X, Chulliat A, Bertrand F, Boness A, Fratter I (2015) A 2015 International Geomagnetic Reference Field (IGRF) candidate model based on Swarm's experimental absolute magnetometer vector mode data. Earth Planets Space 67:95. https://doi.org/10.1186/s40623-015-0265-4

Vigneron P, Hulot G, Léger J-M, Jager T (2018) Geomagnetic field modelling based on ASM-V experimental data. Paper presented at the 8th Swarm Data Quality Workshop, 8–12 October 2018. Frascati, ESA-ESRIN

Vigneron P (2019) Mesures vectorielles expérimentales des instruments ASM de la mission SWARM, du commissioning à la production de modèles de champs géomagnétiques. PhD, Université de Paris, NNT: 2019UNIP7162, available via https://tel.archives-ouvertes.fr/tel-03139970. Accessed 19 Oct 2021

Publisher's Note